PCCP

PCCP

ARTICLE

Gas-Surface Reactions of Nitrate Radicals with Vinyl-terminated Self-Assembled Monolayers†

Yafen Zhang,[a] Robert C. Chapleski, Jr.,[a] Jessica W. Lu,[b] Thomas H. Rockhold, Jr.,[c] Diego Troya [a] and John R. Morris [a]*

Interfacial reactions between gas-phase nitrate radicals, a key nighttime atmospheric oxidant, and a model unsaturated organic surface have been investigated to determine the reaction kinetics and probable reaction mechanism. The experimental approach employs *in situ* reflection-absorption infrared spectroscopy (RAIRS) to monitor bond rupture and formation while a well-characterized effusive flux of NO_3 impinges on the organic surface. Model surfaces are created by the spontaneous adsorption of vinyl-terminated alkanethiols ($HS(CH_2)_{16}CHCH_2$) onto a polycrystalline gold substrate. The $H_2C=CH$-terminated self-assembled monolayers provide a well-defined surface with the double bond positioned precisely at the gas-surface interface. The surface reaction kinetics obtained from RAIRS revealed that the consumption rate of the terminal vinyl groups is nearly identical to the formation rate of a surface-bound nitrate species and implies that the mechanism is one of direct addition to the vinyl group rather than hydrogen abstraction. Upon nitrate radical collisions with the surface, the initial reaction probability for consumption of carbon-carbon double bonds was determined to be $(2.3 \pm 0.5) \times 10^{-3}$. This rate is approximately two orders of magnitude greater than the rate of ozone reactions on the same surface, which suggests that oxidation of surface-bound vinyl groups by nighttime nitrate radicals may play an important role in atmospheric chemistry despite their relatively low concentration.

I. INTRODUCTION

Nitrate radicals (NO_3) are one of the most important oxidizing gases in the atmosphere due to their significant contribution to the degradation of volatile organic compounds (VOC).[1] Interestingly, reactions involving NO_3 occur primarily at nighttime, because NO_3 is rapidly photolyzed to NO/NO_2 during the daytime.[2,3] In addition to reacting with VOCs, NO_3 plays a role in tropospheric chemistry ($\leq$ 10-15 km altitude) by facilitating the formation of HO_x (x=1,2) radicals.[4,5] Further, NO_3 has been implicated as a key intermediate in the formation of certain atmospheric particles, such as secondary organic aerosols.[6,7] Beyond gas-phase reactions, interfacial reactions of NO_3 with atmospheric particles may alter their size, chemical composition, and optical properties.[8,9] Changes in particulate properties affect the scattering and absorption of light, hence shifting the balance between incident and outgoing solar radiation.[10] These key aspects of NO_3 chemistry have motivated

several laboratory studies into the fundamental properties and behavior of this strongly oxidizing molecule.

Following the first reported presence of NO_3 in the troposphere,[11] many studies have focused on gas-phase reactions between nitrate radicals and organic compounds.[6,12-16] NO_3 generation for experimental studies has largely been accomplished by the thermal decomposition of dinitrogen pentoxide (N_2O_5) based on the $N_2O_5 \rightleftharpoons NO_3 + NO_2$ equilibrium.[17,18] Atkinson et al. were among the first to use this method to track the reaction rates of a series of selected organics (e.g. isobutene, benzene) with NO_3 relative to those of reference organics (e.g. ethane, propene) at room temperature.[19] Following these experiments, several other research groups have employed similar relative rate measurements in kinetic studies of gas-phase reactions between NO_3 and atmospheric hydrocarbons.[20-23] In the investigation of the reaction rates involving gas-phase NO_3 and a series of alkenes, Aschmann et al.[20] observed a positive correlation between the measured rate coefficient and the number of carbons within the alkene chain. They attributed this

trend to inductive effects that scale with chain length. That is, the rate of NO_3 addition to the alkene C=C bond increases with the donation of electron density to the C=C bond as provided by additional CH_2 groups.[24] However, for a given number of carbon atoms, they also reported a decrease in reactivity with the extent of branching, which was attributed to steric effects.

Although gas-phase reactions of NO_3 with organics have been widely studied in the laboratory,[19,20,22,25,26] determining the overall rate constants for atmospheric reactions involving NO_3 remains challenging due to difficulties in quantifying the contribution of heterogeneous processes. To help bridge this gap in understanding, Gross et al.[27] studied heterogeneous reactions of NO_3 and N_2O_5 with five different types of organic surfaces. They found the reactive uptake coefficients of NO_3 (the ratio of the number of molecules lost to the surface to the number that collide with the surface) to be about four orders of magnitude higher than those of N_2O_5. These important results suggest that reactions between NO_3 and organics play a larger role in atmospheric chemistry than reactions of N_2O_5. However, due to the lack of a well-defined surface, neither could be quantified with accuracy. To alleviate the problem of not having a well-defined surface in the kinetics experiments involving NO_3 collisions, Gross et al.[28] employed self-assembled monolayers (SAMs).[29-34] They reported that the uptake coefficient for NO_3 on vinyl-terminated SAMs is higher than on liquid or amorphous solid films.[35] This trend likely reflects the differences in the location of the double bonds, which mediates their accessibility to the impinging gas-phase molecules. Interestingly, several expected products (reported in previous gas-phase studies[1,36]) were not observed in their infrared spectroscopic and X-ray photoelectron spectroscopic measurements. This was attributed to the decomposition of products during XPS analysis and to the loss of the species of interest during sample transfer between instruments.[28] Hjorth et al.[37] and Barnes et al.[18] reported organic nitrates as the product of gas-phase reactions of NO_3 with a series of alkenes by characterizing the reaction product with infrared spectroscopy. They found similarities between spectra recorded following their experiments and that of a reference compound, 3-nitrooxy-2-butanone; however, they did not assign these spectral features to specific vibrational modes of the molecules.

Although the studies summarized above revealed that NO_3 reacts efficiently with many types of organic compounds and that the reaction rates depend on the structure of the organic reactant,[27,35,38,39] many important questions remain. In particular, many fundamental aspects of the interfacial chemistry have yet to be investigated, including how surface structure and functionality affect NO_3 reactivity, the nature of major reaction products and the overall reaction mechanisms. In this study, we aim to develop a deeper understanding of the kinetics and pathways for reactions of NO_3 with a vinyl-terminated self-assembled monolayer on gold. SAM surfaces have a number of advantageous properties, including their ordered nature and high reproducibility. They also provide the capability of positioning the carbon-carbon double bond precisely at the gas-surface interface. *In situ* reflection-absorption infrared spectroscopy (RAIRS) was used to monitor NO_3 reactions with the organic

surface. In addition to vibrational spectroscopic studies, X-ray photoelectron spectroscopy (XPS) was implemented to analyze the elemental composition of surface-bound molecules prior to and after reaction with NO_3. By tracking the rate of bond rupture and formation during the gas-surface collision, the initial reaction probability was determined and likely reaction pathways were identified for this important interfacial oxidation reaction.

II. EXPERIMENTAL SECTION

The experiments were performed in an ultrahigh vacuum (UHV) surface science instrument designed for the study of the kinetics and mechanisms of reactions between nitrate radicals and model organic surfaces. The UHV chamber (base pressure of $< 10^{-9}$ torr) eliminates reactions of background gases with the surface and enables the implementation of XPS for elemental characterization of the surface before and after reaction. An all-glass capillary array doser was employed to provide an effusive source of NO_3 radicals that impinge on the surface. The surface-bound species were tracked *in situ* using reflection-absorption infrared spectroscopy (RAIRS), while products that desorb from the surface were monitored with a quadrupole mass spectrometer (QMS) during exposure. A schematic of the instrument is shown in Figure 1.
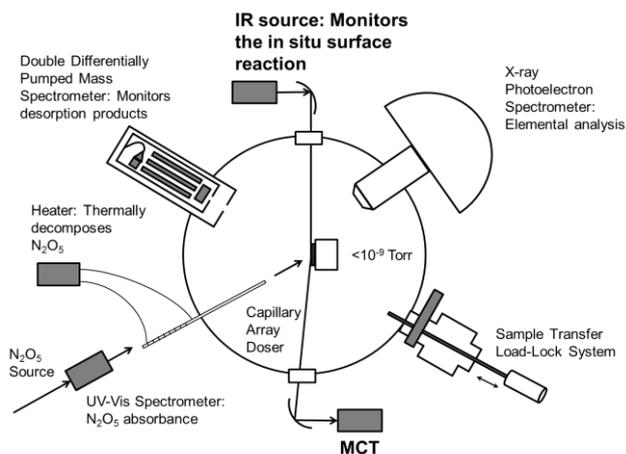
Figure 1. A schematic of the UHV system for surface analysis of NO_3 reactions with vinyl-terminated SAMs. All pre-exposure data were collected at a base pressure of $< 10^{-9}$ torr. N_2O_5 gas molecules are characterized by UV-Vis spectroscopy prior to the thermal decomposition at the doser. *In situ* RAIRS is used to monitor the NO_3 reactions with the organic surface. Other aspects are described in the text.

2.1 Preparation of Vinyl-terminated Self-assembled Monolayers.

The 17-octadecene-1-thiols (18C vinyl-terminated 1-thiol) used in this work were synthesized prior to use according to procedures established by Hu and Fox.[40] The molecules were verified to be >99% pure by ^{1}H NMR measurements. Vinyl-terminated SAMs were created on polycrystalline gold slides which were purchased from EMF Corp. These gold substrates

2 | *Phys. Chem. Chem. Phys.*, 2014, **00**, 1-3

This journal is © The Royal Society of Chemistry 2014

were immersed in a piranha solution (7:3 ratio (v:v), 70% sulfuric acid/30% hydrogen peroxide) for ~1 h to remove surface contamination. The Au surfaces were then removed from the piranha solution and rinsed thoroughly with deionized water (Millipore Purification Systems, 18.2 MΩ). Each substrate was dried with a stream of ultrahigh purity nitrogen (UHP N_2) and immediately placed in a freshly prepared 1 mM solution of 17-octadecene-1-thiol in hexane for at least 24 hours to achieve a well-ordered and densely packed monolayer. The SAMs were then rinsed with hexane and dried under a stream of UHP N_2 before being placed into the UHV chamber through a sample transfer load-lock system.

For benchmark measurements to help with spectral assignments, 2-ethylhexyl nitrate (97%) was obtained from Sigma-Aldrich and used without further purification. A thin film of 2-ethylhexyl nitrate was created by dropping the molecules onto a clean gold surface and then drying the surface under UHP N_2. Following bulk liquid evaporation, a RAIR spectrum was recorded.

2.2 Nitrate Radical Generation.

Nitrogen monoxide (98.5%) was purchased from Sigma-Aldrich and used without further purification. To form NO_3, nitrogen monoxide was oxidized by an excess of ozone. This procedure initially formed N_2O_5 which was introduced into a glass trap submerged in a dry ice/ethanol bath. After isolating the trap from the dry ice/ethanol bath, N_2O_5 was volatilized and delivered to the doser. NO_3 was then formed via thermal decomposition of N_2O_5 upon heating the doser to 324 K. The flux of N_2O_5 onto the surface was estimated from a calculation based on the pressure of N_2O_5 near the doser, the physical dimensions of the doser, and the kinetic theory of gases. According to the temperature-dependent equilibrium constant for $NO_3 + NO_2 \rightleftharpoons N_2O_5$ ($K_{eq} = 2.7 \times 10^{-27} \times \exp(11000K/T)$ cm^3 molecule^{-1}),[41,42] the concentration of NO_3 adjacent to the surface for our doser temperature of 324 K, $[NO_3]_g$, was determined to be 2.8×10^{10} molecules cm^{-3}. The calculated flux was consistent with the pressure change in the vacuum chamber during NO_3 exposure to a clean gold surface.

2.3 Reflection-Absorption Infrared Spectroscopy.

Reactions between NO_3 and SAMs were monitored using a Bruker IFS 66v/S spectrometer attached to the UHV chamber. Focused IR radiation from a SiC globar was reflected from the gold surface at ~86° relative to the surface normal through a differentially pumped KBr window. The reflected radiation was detected by a mid-range (750-4000 cm^{-1}) mercury cadmium telluride (MCT) detector, which was cooled by liquid nitrogen prior to each experiment. All spectra shown here were the average of 100 scans with 2 cm^{-1} resolution.

2.4 X-ray Photoelectron Spectroscopy.

The XPS data presented in this article was obtained by employing monochromatic radiation (Al Kα 1486.6 eV) from a SPECS XR50 X-ray source operating at 250 W (12.5 kV and 20 mA). Ejected photoelectrons were detected using a 16.5" hemispherical energy analyzer (SPECS, Phoibos 100) operated at a take-off angle of 90° with respect to the surface. All high-resolution spectra were acquired in the region of interest using the following experimental parameters: pass energy of 50 eV; step size of 0.1 eV and dwell time of 0.1 s. The binding energy scales for all spectra were referenced to the Au (4f$_{7/2}$) feature at 83.8 eV.[43] A Shirley background was subtracted from each spectrum to account for the inelastic scattering of electrons that contributes to the background broadening.[44,45] The XPS signals are fitted to symmetric curves containing a Gaussian/Lorentzian product with 70% Gaussian and 30% Lorentzian character.[46,47]

2.5 Computational Methods.

Spectral interpretations and mechanistic insight into the reactions were further aided by a series of electronic structure calculations performed using the Gaussian09 code.[48] The geometries of nitrate-terminated linear alkyl radicals with varying carbon-chain length were optimized using both B3LYP/6-31G* and MP2/6-31G* levels of theory, and harmonic vibrational mode analyses were performed on each molecule using both methods. The calculated harmonic frequencies of the scissoring (δ), symmetric stretch (ν_s), and asymmetric stretch (ν_a) normal modes of the nitrate group were found to converge to a constant value with increasing chain length. The relevant vibrational frequencies calculated for each vibrational mode were found to vary by less than 10 cm^{-1} for chains with four or more carbon atoms; therefore, chains with eight carbon atoms were used for the remainder of the computational studies, which provides a balance between accuracy and expense. The appropriateness of this approximation is further evidenced by the agreement of the converged theoretical frequencies (reported in this work for an eight-carbon chain) with those assigned to the 18-C containing SAM employed in the experiments (see Results and Discussion). In addition, to rule out any influence of the anchoring sulfur atom on the vibrational modes under consideration, the vibrational modes of α-SH alkyl chains were compared to those of α-CH$_3$ alkyl chains. The invariance of vibrational frequency (5 cm^{-1} maximum difference) of the modes at the chain terminus with respect to the anchor group demonstrates that the treatment of the anchor group has little influence on our calculations. The majority of the results involving surface models consider the less computationally demanding B3LYP/6-31G* calculations because the converged frequencies on the gas-phase benchmarks are reasonably similar at the B3LYP/6-31G* and MP2/6-31G* levels. All calculated vibrational frequencies reported in this work have been scaled by the recommended factors of 0.96 for B3LYP/6-31G* and 0.94 for MP2/6-31G*.[49]

This journal is © The Royal Society of Chemistry 2014

Phys. Chem. Chem. Phys., 2014, **00**, 1-3 | **3**

III. RESULTS AND DISCUSSION

The reaction dynamics and kinetics that govern the interactions between NO_3 and model organic surfaces have been investigated by tracking interfacial bond formation and rupture with infrared spectroscopy. Vinyl-terminated self-assembled monolayers provide a well-characterized model surface with the double bond positioned precisely at the gas-surface interface. Upon NO_3 collision with the SAM, the molecules could either react with the terminal vinyl groups or simply desorb into vacuum. For those molecules that react, the probability for reactions, γ = number of reactions/number of total collisions, was determined from the kinetics for vinyl group decomposition and new product formation during exposure to a constant flux of nitrate radicals. The kinetics of bond rupture and formation were tracked with *in situ* reflection-absorption infrared spectroscopy while the reaction products were analyzed with RAIRS and XPS.

3.1. Initial H₂C=CH-SAM Characterization by RAIRS.

The model hydrocarbon surface chosen for this work was an 18C vinyl-terminated SAM. The reasons for selecting a long-chain SAM were threefold: (*i*) the thermodynamic stability of SAMs increases with the length of the chains, (*ii*) long-chain (n>10) SAMs are more ordered than short-chain SAMs, and (*iii*) oxidation of S attached to Au does not occur within the time scale of our measurements for the long-chain vinyl-terminated SAM. Further, the C=C stretch of the vinyl group has a strong transition dipole moment that facilitates detailed infrared spectroscopic studies of this mode as it transforms from reactant into product.

Infrared spectra, recorded prior to NO_3 exposure, revealed that the long-chain vinyl-terminated alkanethiols formed well-ordered monolayers on the gold substrates employed in these studies. Figure 2 shows the reflection-absorption infrared spectrum of an 18C vinyl-terminated SAM on a polycrystalline gold substrate. The most intense bands at 2918 and 2849 cm⁻¹ are due to the asymmetric ($\nu_a(CH_2)$) and symmetric ($\nu_s(CH_2)$) stretching modes of CH_2 groups along the backbone of the chains. Both the position and the width of the two bands suggest that the chains reside in a crystalline-like environment.[31,34] An extensive discussion of RAIRS characterization for SAMs can be found in references 50 and 51. In addition to the methylene stretching modes, six of the bands associated with the terminal vinyl group appear in the spectrum of Figure 2. The bands at 3084 and 2984 cm⁻¹ are attributed to the asymmetric ($\nu_a(=CH_2)$) and symmetric CH_2 ($\nu_s(=CH_2)$) stretching modes of the $=CH_2$ group.[52] The four other spectral features at 3008, 1644, 994 and 914 cm⁻¹ are due to the β C-H stretch of -HC=CH₂ (ν(H-C=CH₂)), the C=C stretch (ν(C=C)), the C=C out-of-plane deformation (C=C$_{oop\ def}$), and the $=CH_2$ out-of-plane deformation ($\omega(=CH_2)$), respectively.[53,54] The wavenumbers and corresponding mode assignments for the RAIR spectrum are provided in Table I. The consistency of the features in this characteristic spectrum with previous studies suggests a 21.4 Å² occupation of a single alkenethiol chain adsorbed on the gold substrate, which corresponds to a surface density of 4.7 X 10¹⁴ molecules cm⁻².[29,34]
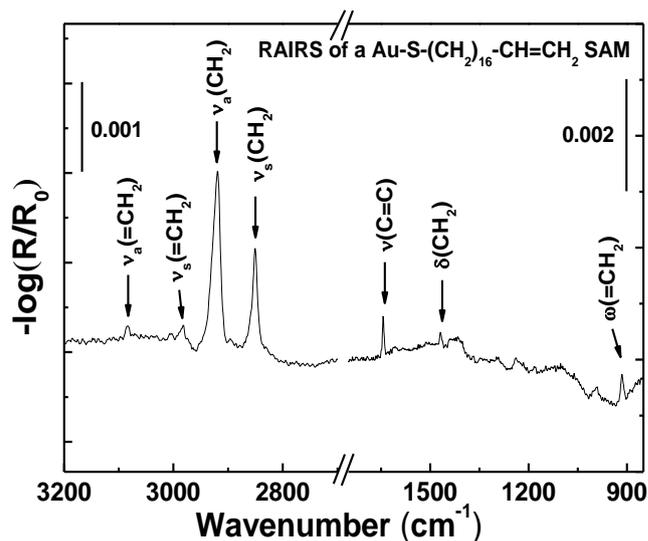
Figure 2. Reflection-absorption infrared spectrum of a H₂C=CH-SAM on Au formed from an 18C vinyl-terminated alkenethiol fabricated through solution immersion. The four most intense IR active modes are highlighted as $\nu_a(CH_2)$, $\nu_s(CH_2)$, ν(C=C), and ω(=CH₂).

Table I. RAIR spectroscopic band positions and vibrational mode assignments for an 18C vinyl-terminated SAM on Au and the vinyl-terminated SAM after NO_3 exposure.

Vibrational Modes	Wavenumber (cm⁻¹)		References
	Pre Exposure	Post Exposure	
$\nu_a(=CH_2)$	3084	-	52-54
ν(H-C=CH₂)	3008	-	52-54
$\nu_s(=CH_2)$	2984	-	52-54
$\nu_a(CH_2)$	2918	2919	31, 35
$\nu_s(CH_2)$	2849	2850	31, 35
$\nu_a(-ONO_2)$	-	1649	28, 55-57
ν(C=C)	1644	-	52-54
$\nu_s(-ONO_2)$	-	1280	28, 55-57
C=C$_{oop\ def}$	994	-	52-54
$\omega(=CH_2)$	914	-	52-54
$\delta(-ONO_2)$	-	857	28, 55-57

4 | *Phys. Chem. Chem. Phys.*, 2014, **00**, 1-3

This journal is © The Royal Society of Chemistry 2014

3.2. IR Characterization of H₂C=CH-SAMs during NO₃ exposure.

Oxidation of the H₂C=CH-SAM by NO₃ was monitored *in situ* by RAIRS. Fig. 3A shows a subset of RAIR difference spectra for the 18C vinyl-terminated SAM during NO₃ exposure. Following the initial characterization, the vinyl-terminated SAM was exposed to a continuous source of NO₃/NO₂ gas. In this experiment, the original SAM was used as the background such that negative features in the spectra indicate the removal of modes from the surface and positive bands reveal an increase in absorbance or the development of new modes. The initial spectrum in Fig. 3A (the lower-most spectrum) is the difference spectrum of the monolayer before exposure. From the bottom toward the top of this figure, the exposure of the monolayer to NO₃ increases by 2×10^2 L (1 Langmuir (L) = 10^{-6} Torr·s) per scan with a total exposure of 5×10^3 L of NO₃. Control experiments performed by exposing an 18C vinyl-terminated SAM to an effusive room-temperature flux of N₂O₅ (without heating the nozzle) or pure NO₂ displayed little or no evidence (spectral changes can be barely observed above noise) for reactions on the time scale shown in Fig. 3. In addition, the exposure of an 18C CH₃-SAM to the NO₃-rich source resulted in only minor changes in the difference IR spectra. For exposure of the H₂C=CH-SAM to the NO₃-rich gas source, three notable changes in the RAIR difference spectra are apparent: (*i*) all of the bands associated with the double bond decrease in intensity, (*ii*) new modes emerge at 1649 cm⁻¹, 1555 cm⁻¹, 1280 cm⁻¹ and 857 cm⁻¹, and (*iii*) the bands associated with the methylene backbone of the SAM broaden and shift to higher wavenumbers, and the intensities decrease by ~10%. As discussed below, these spectral changes are attributed to reactions of NO₃ at the vinyl group. The identities of key products in this reaction have been determined through spectral assignments of the IR modes and analysis of electron binding energies (XPS).

As mentioned above, commensurate with a decrease in the absorbance for the modes associated with the C=C group, positive features emerge in the spectra at 1649 cm⁻¹, 1555 cm⁻¹, 1280 cm⁻¹, and 857 cm⁻¹. Previous infrared spectroscopic studies of the vibrational modes of nitro groups in aromatic and aliphatic nitro organics showed an asymmetric stretch of NO₂ near 1555 cm⁻¹, which suggests that the feature observed (Fig. 3) at this frequency is most likely due to the asymmetric NO₂ stretch of nitro compounds.[55,56] The formation of nitro-containing organics is likely due to addition of NO₂ to the alkyl radical formed upon addition of NO₃ to the double bond.[1] Other mode assignments were aided by the creation of a reference sample composed of a thin film of 2-ethylhexyl nitrate (C₄H₉CH(C₂H₆)CH₂ONO₂) on gold. The RAIR spectrum for this thin film is displayed in Figure 3C (red line). For comparison, an infrared spectrum for an 18C vinyl-terminated SAM after 5000 L of NO₃ exposure (with the original SAM as the background) is also exhibited in Figure 3C (black line). The coincidence of bands at 1649 cm⁻¹, 1280 cm⁻¹ and 857 cm⁻¹ for the two spectra suggests that organic nitrates similar to those in 2-ethylhexyl nitrate are created during exposure of the H₂C=CH-SAM to NO₃. This result corroborates previous results obtained during studies of NO₃ reactions with unsaturated alcohols, which reported the appearance of infrared bands at 1678 cm⁻¹, 1285 cm⁻¹ and 842 cm⁻¹ in FTIR.[57] Other investigations into reactions between NO₃ and an 11C vinyl-terminated SAM also showed evidence for product formation that yielded spectral signatures similar to those displayed in Figure 3.[28] We note that, the relative intensity of the band at 1649 cm⁻¹ is lower than the analogous IR signal recorded for the reference sample (See Fig. 3C). This difference may be due to the surface selection rule, which limits the infrared transition probability by the magnitude of the transition dipole moment component that lies in a direction perpendicular to the plane of the surface.[31,51]

To further aid the interpretation of the IR signal that emerges during exposure, a series of electronic structure calculations were performed (see Sect. 2.5). For these calculations, a SAM model was constructed consisting of a central ω-ONO₂ octyl radical chain surrounded by 36 8C vinyl-terminated chains arranged as they are on the self-assembled monolayer utilized in the experiment (hexagonal arrangement with each chain occupying 21.4 Å² surface area). Because full *ab initio* calculations of this SAM model are prohibitive, a multilevel quantum mechanics/molecular mechanics (QM:MM) approach was used. In this QM:MM approach, the central, ω-ONO₂ alkyl radical, chain was optimized at the B3LYP/6-31G* level, and the rest of the SAM was computed at the MM level with the universal force field (UFF).[58] To test the reliability of the model, calculations were repeated using a modified AMBER force field[59] for the MM region (see Supporting Information for details). Finally, deleterious edge effects in the SAM model were prevented by fixing the outermost boundary of ω-vinyl chains and all the α carbons during the geometry optimization. Fig. 3B shows the construction and optimization strategy of this QM:MM system and the blue trace in Fig. 3C represents the vibrational spectrum of the central radical chain. The very close agreement between the theoretically calculated vibrational spectrum for the nitrate terminus of the SAM model and the experimental IR spectrum verifies that the most likely assignments for the key bands during NO₃ reactions with the H₂C=CH-SAM are the asymmetric and symmetric NO₂ stretches and the NO₂ scissoring of organic nitrates.

This journal is © The Royal Society of Chemistry 2014

Phys. Chem. Chem. Phys., 2014, **00**, 1-3 | 5
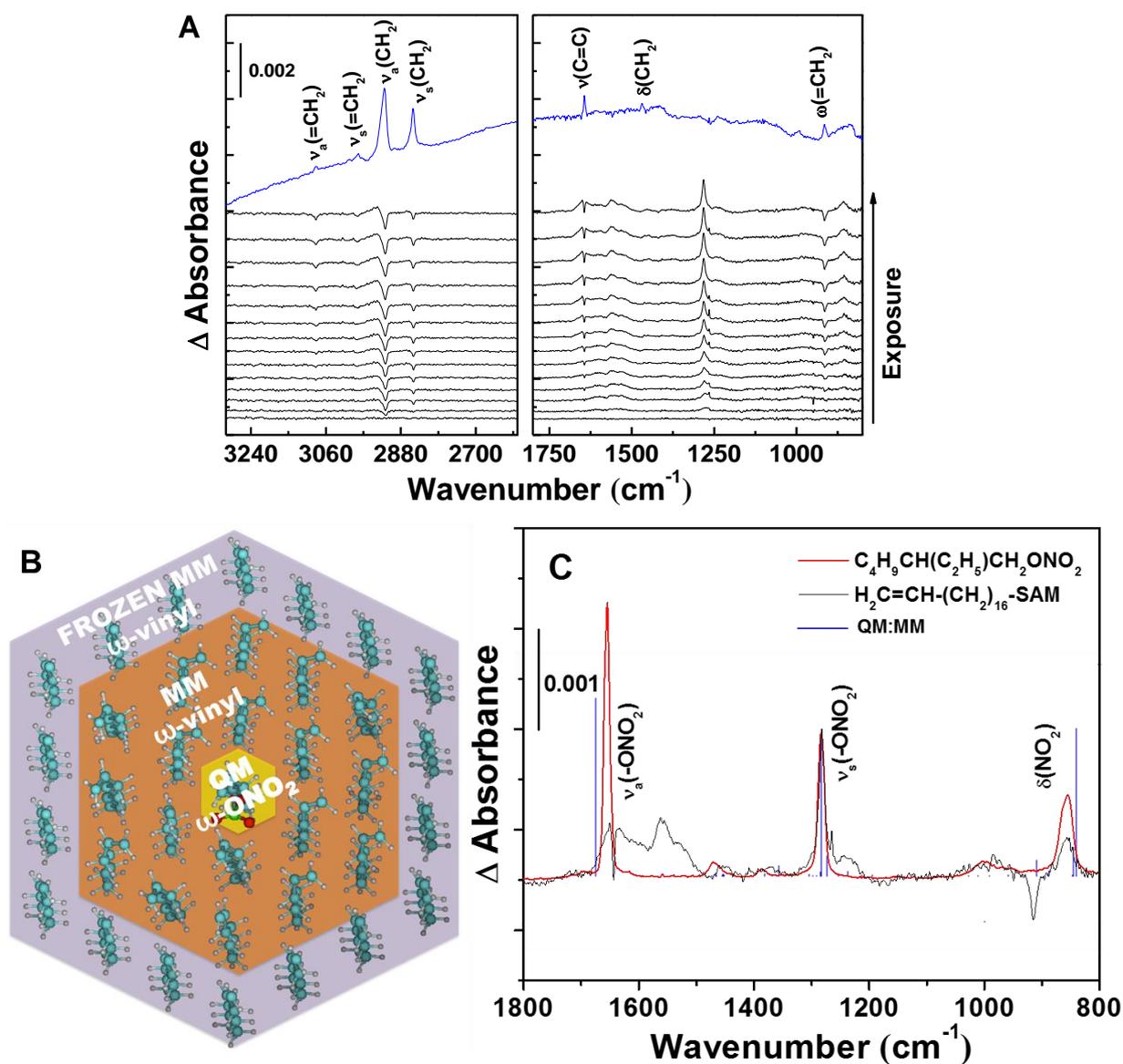
Figure 3. (A) Reflection-absorption infrared difference spectra of an 18C vinyl-terminated SAM exposed to NO$_3$. The spectrum shown on top in blue is that of the SAM prior to NO$_3$ exposure using a clean Au sample as the background. Upon NO$_3$ exposure, the spectra in black show that modes associated with the C=C moiety decrease and new modes emerge. The background for this scan is the original pre-exposure spectrum (blue), with the exposure increasing by 2 X 10^2 L per spectrum. (B) Schematic of the model SAM used in the QM:MM calculations of this work. (C) RAIR spectra of a 2-ethylhexyl nitrate surface (red), an 18C vinyl-terminated SAM after 5000 L of NO$_3$ exposure (black), and theoretical QM:MM frequencies (blue) of the central ω-ONO$_2$ radical chain.

Table II lists the vibrational frequencies relevant to the experiments in this work. Interestingly, the table shows that the largest difference between gas-phase and SAM models in the electronic structure calculations is only 10 cm^{-1} at the same level of theory. The fact that the ω-ONO$_2$ vibrational modes differ only modestly between the gas-phase and the SAM model indicates that embedding a nitrate alkyl chain in a SAM has very little effect on the nitrate vibrational frequencies.

6 | *Phys. Chem. Chem. Phys.*, 2014, **00**, 1-3

This journal is © The Royal Society of Chemistry 2014

Table II. Experimental ω-ONO₂ octadecyl SAM and theoretical gas-phase and SAM ω-ONO₂ octyl chain vibrational frequencies (cm⁻¹)

Methods	δ(-ONO$_2$)	ν_s(-ONO$_2$)	ν_a(-ONO$_2$)
Experiment	857	1280	1649
B3LYP/6-31G* (gas-phase)	831	1275	1673
MP2/6-31G* (gas-phase)	825	1234	1750
Multilevel SAM (B3LYP/6-31G*:UFF)	841	1283	1673
Multilevel SAM (B3LYP/6-31G*:Amber)	834	1277	1673

Beyond the spectral changes observed in the low wavenumber region (1800-800 cm⁻¹) and the decrease in the intensity of stretching modes associated with the double bonds at high wavenumbers (>3000 cm⁻¹), the only changes observed in the difference spectra (above the detection limit of the spectrometer, which we estimate to be 2% of a ML) are the decrease in intensities, the broadening, and the blue shift of bands assigned to the asymmetric and symmetric stretching modes of the CH₂ groups along the backbone of the chains. Typically, the frequency of the asymmetric and symmetric CH₂ stretching modes falls at 2918 cm⁻¹ and 2849 cm⁻¹, respectively, in tightly packed well-ordered monolayers.[31] Relatively disordered organic films exhibit stretching modes at much higher vibrational energy.[33] Therefore, the blue shift of these two modes for methylene chains observed in Fig. 3A indicates that the well-ordered SAMs become increasingly disordered as the terminal groups react with impinging NO₃. In addition, as the local environment becomes less homogeneous, the substantial broadening of the two bands was observed. Therefore, the addition of a bulky nitrate group to the end of the alkane chain likely leads to disordering of the originally well-ordered SAM, which could result in the broadening and the blue shift of the bands assigned to the methylene stretching modes. In addition, the decrease in the absorptivity for the features assigned to C-H stretches along the methylene backbone might be due to hydrogen abstraction to form HNO₃, which has been reported in previous studies of NO₃ reactions with organics.[6,60,61] However, any HNO₃ (g) that may have been produced was below the limit of detection of our quadruple mass spectrometer.

3.3. XPS Characterization.

While infrared spectroscopy provides insight into the vibrational motions of adsorbed products, the elemental composition of the adsorbates can be effectively analyzed with XPS. Elemental analysis was performed prior to and after reactions of the vinyl-terminated SAM with NO₃. Representative high resolution spectra of the N (1s), S (2p), O (1s) and C (1s) regions of an 18C vinyl-terminated SAM are shown in Figure 4.

The high resolution XPS data collected in the N (1s) region of the SAM surface before and after NO₃ exposure are shown in Figure 4A. The N (1s) spectrum of the surface-bound product after reactions was fit best by a model containing three components with equal full-width-at-half-maximum (FWHM) values. The best fit required a FWHM value of 1.8 eV, which is similar to the values found in a number of XPS studies of nitrates adsorbed at different metal surfaces.[46,47,62-64] The agreement of the binding energy at 406.9 eV in the N (1s) region in this work with that from previous XPS studies of nitrate adsorbates further demonstrates the formation of an organic nitrate group during reactions between the vinyl-terminated SAM and NO₃. In addition, upon prolonged exposure of NO₃ to an 18C methyl-terminated SAM, no XPS signal above the noise in the region of organic nitrates was detected. Therefore, we conclude that the feature at 406.9 eV is most likely assigned to the nitrogen in organic nitrates. Two additional and much weaker features are present in the spectrum centered at 405.5 eV and 408.8 eV. Similar features at nearly the same binding energies have been observed in several previous studies in which they were assigned to physisorbed NO₂ (405.6 eV) or NO₃⁻ adsorbates (408.1 eV).[46,47] A summary of the binding energies compared to literature values is provided in Table III.[46,47,62-64] It should be noted that the organic nitrates were found to be highly unstable when exposed to X-rays and the intensity of the signal at the N (1s) binding energy decayed rapidly with exposure. Subsequent experiments have also shown that the surface-bound product decomposes upon visible-light exposure, a topic that will be explored in future studies.

As the vinyl groups are converted to nitrate-containing products, a signal corresponding to the binding energy for O (1s) electrons also emerges in the high resolution XPS spectra (see Fig. 4C). As expected, the vinyl-terminated monolayer shows no signal above noise for the O (1s) transition before exposure. After 5000 L of NO₃ exposure, a feature positioned at 531.6 eV is consistent with that observed for AgNO₃ at 532.2 eV, and for adsorbed nitrates on a silver surface at 531.6 eV.[62] Interestingly, the FWHM of the electron signal in the O (1s) region is larger than that for previous studies of surface-adsorbed nitrates,[47,62-64] indicative of a more diverse chemical environment for oxygen that may arise from nitro- as well as nitrate-containing surface-bound products.

This journal is © The Royal Society of Chemistry 2014

Phys. Chem. Chem. Phys., 2014, **00**, 1-3 | **7**
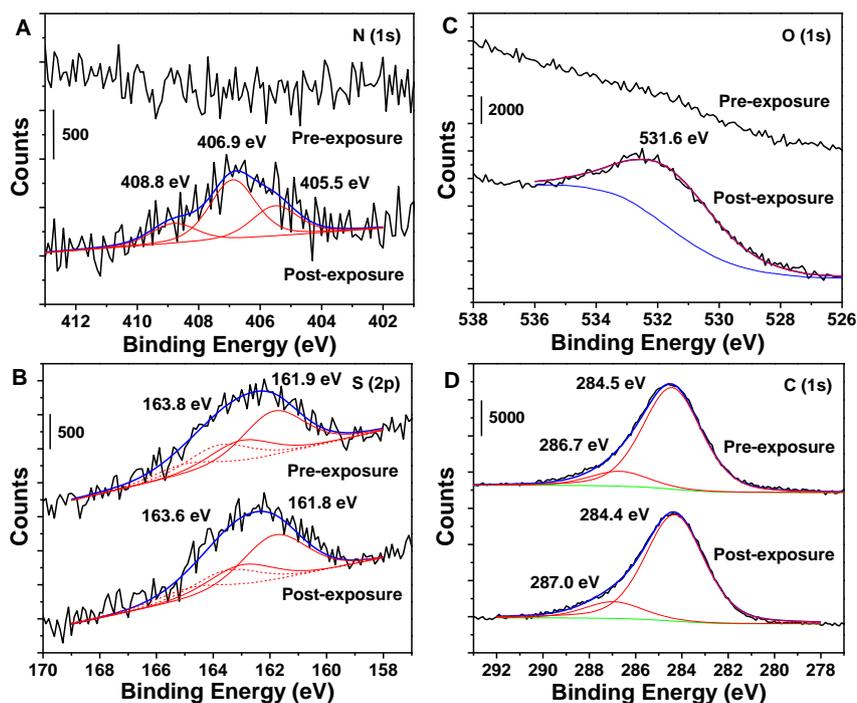
Figure 4. High resolution X-ray photoelectron spectra of the N (1s), S (2p), O (1s), and C (1s) regions of an 18C vinyl-terminated SAM before and after 5000 L of NO₃ exposure, which indicates the formation of organic nitrates and preservation of concentration and oxidation state of sulfur g roups attached to the Au surface.

Table III. Comparison of binding energies for N (1s) transitions for several nitrogen-compounds

Species	Binding Energy (eV)	
	N (1s)	
	This Work[a]	Literature Reference[b]
-ONO₂	406.9	407.3, 407.2, 405.7 [46] Baltrusaitis et al., [63] Vovk et al., [62] Zemlyanov et al.
NO₃⁻		407.5 [47] Rosseler et al.
AgNO₃		406.2 [62] Zemlyanov et al.
NaNO₃		407.4 [46] Baltrusaitis et al.
NO₂, NO₃	405.5, 408.8	405.9, 409.5, 405.4, 407.6 [46] Baltrusaitis et al., [47] Rosseler et al., [64] Ammann et al.

[a] Calibrated to the Au (4f₇/₂) feature at 83.8 eV. [b] Baltrusaitis et al. C (1s) at 285.0 eV; Vovkc et al. calibration not specified; Zemlyanov et al. and Rosseler et al. Au (4f₇/₂) at 84.0 eV; Ammann et al. O (1s) of gas-phase water at 539.7 eV

The N (1s) spectra revealed that oxidation of the vinyl-terminated SAM by NO₃ resulted in the formation of nitrate compounds. However, in addition to the vinyl terminus, the Au-S bond is susceptible to oxidation, which would complicate interpretation of the IR results. Fortunately, XPS spectra of the S (2p) electrons before and after NO₃ exposure show that concentration and oxidation state of sulfur are unaffected by the impinging gas. The XPS data (Fig. 4B) has been fitted to a composite (blue line) of two pairs of S (2p₃/₂,₁/₂) with the same FWHM, branching area ratio of 2 (2p₃/₂:2p₁/₂), and standard spin-orbit splitting of 1.2 eV (the S (2p₃/₂) feature at 161.9 eV and an irradiation-induced sulfur species S (2p₃/₂) feature at 163.8 eV).[43,65,66] After 5000 L of NO₃ exposure, similar doublets are observed with nearly the same intensity,[67] which reveals that few, if any, Au-S bonds have been oxidized during the NO₃ exposure. Thus, reactions for this study appear to be isolated to the vinyl groups at the chain terminus. The preservation of the SAM is also evidenced by the high resolution XPS spectra in the C (1s) region (see Fig. 4D). The features centered at 284.5 eV and 286.7 eV are coincident with the binding energy of the C (1s) electron in regular methylene groups and in the carbon atoms bound to sulfur.[65,68,69] After NO₃ exposure, the intensity of the electron signal at 284.4 eV was preserved, indicating that, in agreement with RAIRS data, few methylene chains desorbed from the surface upon reaction. In addition, the shoulder positioned at 287.0 eV suggests the emergence of a C-O or C=O species on the surface and is likely related to the carbon adjacent to the nitrate group that forms during oxidation of the double bond to yield a C-ONO₂ group.[47,67,70]

8 | *Phys. Chem. Chem. Phys.*, 2014, **00**, 1-3

This journal is © The Royal Society of Chemistry 2014
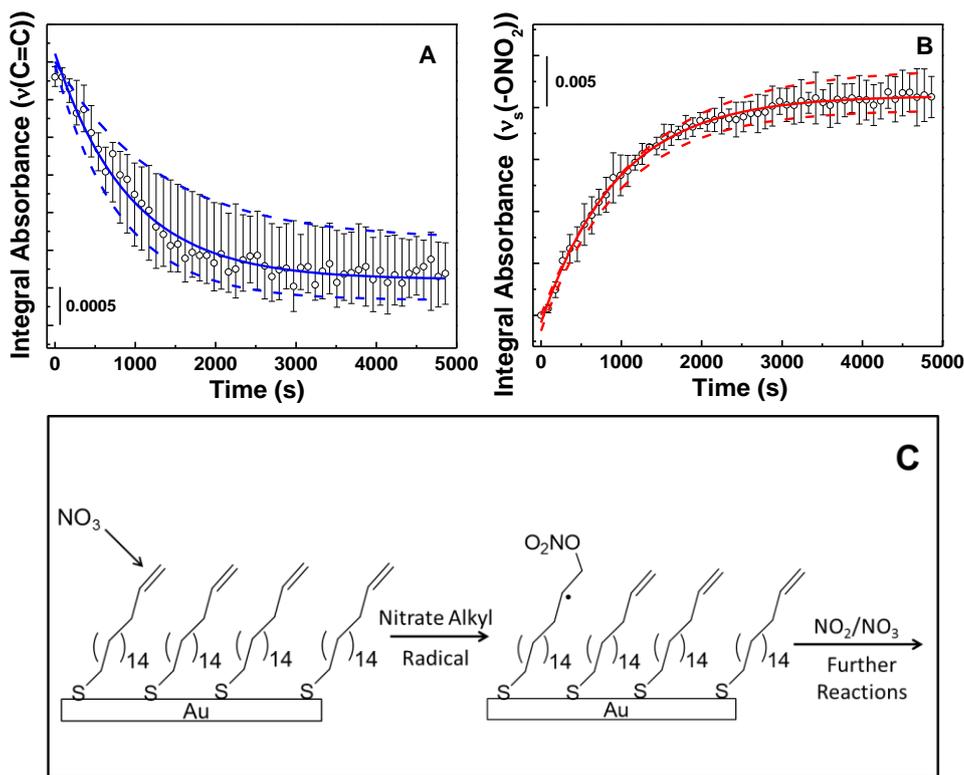
Figure 5. (A) Integrated absorbance for $\nu(C=C)$ (at 1644 cm^{-1}) versus time during NO$_3$ exposure. The lines are the best fit for Equation (1). (B) Integrated absorbance for $\nu a(-ONO_2)$ (at 1280 cm^{-1}) versus time during NO$_3$ exposure. The lines are the best fit for Equation (2). (C) A scheme of the possible mechanistic pathways showing the addition of NO$_3$ to the carbon-carbon double bond and the formation of an alkyl nitrate radical.

3.4 Reaction rate, probability and proposed mechanism.

The preceding results provide evidence for the formation of an organo-nitrate species during the collisions of NO$_3$ on the vinyl-terminated SAM. The overall reactivity of NO$_3$ with the vinyl-terminated SAM is characterized by the reaction probability, which can be determined from the reaction rates.[27,39,71] The integrated intensities of the infrared bands assigned to the C=C mode at 1644 cm^{-1} and the asymmetric NO$_2$ stretch of organic nitrates at 1280 cm^{-1} are shown as a function of time during NO$_3$ exposure in Figure 5A and 5B. The lines through the data show that the rate of change for these IR features track pseudo-first-order kinetics, which follows a single exponential trend characterized by the rate constants k_{obs} = (1.4 ± 0.3) X 10^{-3} s^{-1} and k_{obs}' = (1.3 ± 0.2) X 10^{-3} s^{-1} according to the following equations:

$$A_{1644}(t) = (A_{1644})_0 \exp(-k_{obs} t) \qquad (1)$$

$$A_{1280}(t) = (A_{1644})_0 [1-\exp(-k_{obs}' t)] \qquad (2)$$

where $A_{1644}(t)$ is the absorbance of the C=C group, $(A_{1644})_0$ is the initial absorbance of the same group before exposure to NO$_3$, and $A_{1280}(t)$ is the absorbance of the asymmetric NO$_2$ stretch of organic nitrates at 1280 cm^{-1}. The similarity of the two rate constants demonstrates a strong correlation between consumption of the double bonds and production of surface-bound nitrates.

The overall reaction probability, reflected by the rate of change in the IR intensity of the vinyl group, decreases with time as surface sites are consumed. The reaction probability for NO$_3$ impinging on the vinyl-terminated SAM depends on the rate constant, the surface coverage of reactive sites and the flux of NO$_3$. The initial reaction probability, γ_0, was determined by Equation (3)[72]

$$\gamma_0 = 4\theta_{max} k_{obs} /(<v> [NO_3]_g) \qquad (3)$$

where $<v>$ is the mean molecular velocity of gas-phase NO$_3$, $[NO_3]_g$ is the gas-phase NO$_3$ concentration adjacent to the surface, t is the time of exposure to NO$_3$, and θ_{max} is the initial surface coverage of the carbon-carbon double bonds. The initial reaction probability for NO$_3$ collision with the 18C vinyl-terminated SAM is γ_0 = (2.3 ± 0.5) X 10^{-3}. That is, we find that approximately two reactions occur in every ~1000 collisions between NO$_3$ and the carbon-carbon double bonds.

The initial reaction probability for NO$_3$ on the vinyl-terminated SAM is an order of magnitude smaller than the uptake coefficient for NO$_3$ on unsaturated fatty acid particles, as reported by Zhao et al.[39] Similarly, higher reaction probabilities have been measured for NO$_3$ on alkenoic acids in a cylindrical flow reactor by Gross et al.[27] In addition, Bertram et al. reported a reaction probability of 3.4 X 10^{-2} for NO$_3$ exposure to an 11C vinyl-terminated SAM.[28] These previous studies differ from the work presented here in two important ways. First, in the previous work, the NO$_3$ consumption rate (rather than the rate of product formation) during the reaction was employed to determine the

reaction probability. Secondly, the work by Bertram et al. was conducted in the presence of O_2 (rather than a clean vacuum environment). O_2 may play a role in the overall chemistry by oxidizing the alkyl radical to produce a nitroxy peroxyl radical that would undergo additional reactions with NO_3.[28] Thus, comparisons between the reaction rate reported here and those in the previous studies by Bertram et al. suggest that background gases play a critical role in the overall chemistry under real-word conditions.

During the heterogeneous oxidation of the vinyl-terminated SAM by NO_3 studied here, we observed that all of the bands associated with the double bond decreased in intensity at identical rates and concurrently with the emergence of new modes at 1649 cm^{-1}, 1280 cm^{-1} and 857 cm^{-1}, which are attributed to the formation of organo-nitrate moieties. The new features observed in RAIRS are consistent with the emergence of N (1s) and O (1s) electrons in the high-resolution XPS energy distributions. These results suggest that the reaction mechanism is one of addition to the vinyl group, such as: $NO_3\cdot + H_2C=CH-(CH_2)_{16}SAu \rightarrow O_2NO-CH_2- \cdot CH-(CH_2)_{16}SAu$. The addition likely occurs in such a way as to generate a radical in the subterminal C atom of the SAM, which is thermodynamically more favorable than its generation on the less substituted terminal C atom, as shown in Figure 5C. In addition, the bands associated with the methylene backbone of the SAM broadened and decreased slightly in intensity, which could be due to many related processes. Specifically, propagation or reaction of the alkyl radicals would likely alter the configuration of the SAM and reorientation of the methylene backbone may occur if additional impinging NO_3 or NO_2 adds to the alkyl radical.

The experimental results suggest that NO_3 adds exclusively to the terminal vinyl group and we have little evidence for the hydrogen abstraction reaction, $NO_3\cdot + H_2C=CH-(CH_2)_{16}SAu \rightarrow \cdot CH=CH-(CH_2)_{16}SAu + HNO_3$, which would be inconsistent with the type of first-order kinetics observed. This result is contrary to previous studies that highlight the important role that abstraction plays in nitrate-hydrocarbon chemistry.[1,6,60,61] To gain further insight into this result, we have conducted high-level electronic structure calculations of both the addition and the hydrogen abstraction reaction channels for NO_3 collision with vinyl groups by using propene as a model substrate. CCSD(T)/aug-cc-pVDZ single-point calculations employing B3LYP/6-31G* geometries indicate that the $NO_3\cdot + H_2C=CH-CH_3 \rightarrow \cdot CH=CH-CH_3 + HNO_3$ hydrogen abstraction reaction is endothermic by 8.3 kcal/mol and has a barrier of 9.9 kcal/mol. Under the thermal conditions of the experiment, only a very small fraction of NO_3 molecules possess enough energy above the hydrogen abstraction barrier. This result provides a thermodynamic justification for the lack of apparent hydrogen abstraction reactions in the collisions of NO_3 with the vinyl-terminated SAMs examined in this work. Regarding the addition reaction, $NO_3\cdot + H_2C=CH-CH_3 \rightarrow O_2NO-CH_2- \cdot CH-CH_3$, electronic structure calculations at the same level (CCSD(T)/aug-cc-pVDZ//B3LYP/6-31G*) indicate this reaction is exothermic by 19.1 kcal/mol. However, the B3LYP/6-31G* calculations failed to locate a transition state.

Consequently, we attempted to characterize the region of the potential energy surface (PES) that connects reagents with the transition state by scanning the C-O bond that is formed during the reaction from the addition minimum to the reagents' asymptote. The remaining coordinates were fully relaxed during the scan. Figure 6 shows that (as anticipated from the inability to locate a transition state using conventional methods) the B3LYP/6-31G* method predicts a continuously downhill reaction path (black line). Single-point energies with the B3LYP/6-31G* geometries using other density functionals with larger basis sets also corroborate this observation, as illustrated in Fig. 6. In addition, while using the B3LYP/6-31G* method to scan geometries directly, we utilized CCSD(T)/aug-cc-pVDZ at selected points during the scan to provide a higher-level description of the reaction path (blue line). As with the rest of methods used in this work, CCSD(T)/aug-cc-pVDZ also predicts the absence of a barrier for the addition reaction. These calculations clearly indicate that addition is kinetically more favored than abstraction which requires surmounting a significant barrier.
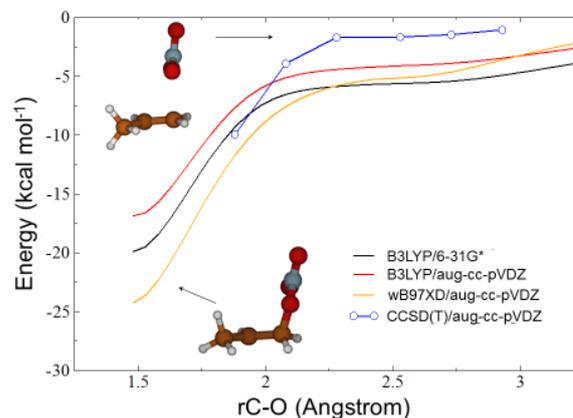
Figure 6. Potential-energy surface scan of the C-O coordinate for the addition reaction of NO_3 to propene. All calculations have been carried out with B3LYP/6-31G* geometries. Energies have not been zero-point corrected.

Interestingly, the initial reaction probability reported here, γ_0 = (2.3 ± 0.5) X 10^{-3}, is approximately two orders of magnitude higher than that for the reaction of ozone with long-chain vinyl-terminated SAMs (studied in the same laboratory).[53] One of the factors that might contribute to the origin of this difference in reactivity is that the energetic requirements for ozone addition might be larger than those of nitrate addition. To illuminate this point, we have calculated the barrier for O_3 addition to propene at the same CCSD(T)/aug-cc-pVDZ//B3LYP/631-G* level with which we characterized the NO_3 addition reaction. These calculations show that the barrier for ozone addition is below the reagents' asymptote (-1.9 kcal/mol, including zero-point correction). This result, which implies that both nitrate and ozone addition to propene are barrierless, does not explain the two-orders-of-magnitude difference in the measured reaction probabilities.

A difficulty in using these calculated barriers to explain differences in reactivity is that they correspond to gas-phase models, in which the minimum energy approach of NO_3 or O_3 to

10 | *Phys. Chem. Chem. Phys.*, 2014, **00**, 1-3

This journal is © The Royal Society of Chemistry 2014

the double bond is not impaired by neighboring molecules. Along the minimum energy path, the NO_3 molecules approach perpendicularly to the double bond, so that the new C-O bond is perpendicular to the double bond (see insets of Figure 6). For ozone addition, two C-O bonds must form perpendicular to the double bond to yield a cyclic primary ozonide.[73] Molecular dynamics simulations show that in a vinyl-SAM, the terminal double bond has a distribution of orientation at ambient conditions in which the double bond is rarely, if at all, perpendicular to the incoming NO_3 and O_3 molecules. Instead, the double bond tends to lie predominantly more parallel to the surface normal, implying that the perpendicular transition state obtained in the gas-phase calculations is not readily accessible in the first collision of the gases with the surfaces under our experimental conditions. Instead, reactions are likely caused by NO_3 and O_3 molecules trapped on the surface that encounter thermally fluctuating double bonds in geometries appropriate for reaction. Since the addition of NO_3 to the terminal double bond requires the formation of a perpendicular O-C bond with only the terminal C atom of the vinyl group, but O_3 addition requires the simultaneous formation of two O-C bonds with the terminal and the subterminal C atoms of the double bond, the probability of thermally sampling the transition state region for nitrate addition may be far more likely than for ozone addition. These differences in the relative accessibility of the reaction coordinate are likely responsible for the larger interfacial reaction probability for nitrate radical observed in our experiments. This result is likely a general phenomenon that extends to other organic surfaces and may help to account for the overall shorter lifetime of atmospheric NO_3 relative to O_3.

IV. SUMMARY

The exploration of the oxidation of surface vinyl groups by NO_3 investigated in this work reveals insight into three key aspects of this reaction. First, surface vinyl groups are consumed at the same rate as organic nitrate formation, suggesting that the consumption of vinyl groups is primarily responsible for the formation of organic nitrates. Second, the initial reaction probability, $(2.3 \pm 0.5) \times 10^{-3}$, is approximately two orders of magnitude higher than that for the reaction of ozone with the same SAM, which is likely due to the higher accessibility of the transition state for nitrate addition. The proposed mechanism begins by initial addition of NO_3 to the carbon-carbon double bonds to form an alkyl nitrate radical that may undergo subsequent reactions, such as NO_2 addition. Even under long exposure time, there is little indication of sulfur oxidation, suggesting that the reactions were limited to the terminal groups. Together, these insights may influence the development of more accurate theoretical models to understand the detailed kinetics and dynamics of NO_3 reactions with atmospheric organics for predicting the fate of NO_3 in the environment. Ultimately, future work exploring reactions of mixed SAMs that contain polar functional groups may further the understanding of the importance of interfacial functionality in determining the fate of

gas-surface collisions involving NO_3 radicals on secondary organic aerosols in the atmosphere.

Notes

* Corresponding Author: jrmorris@vt.edu

Tel: (540)231-2472.

[a] Department of Chemistry, Virginia Polytechnic Institute and State University, Blacksburg, VA 24061, USA.

[b] Laboratory of Physical Chemistry, ETH Zürich, Vladimir-Prelog-Weg 2, CH-8093, Zürich, Switzerland.

[c] Virginia Department of Transportation - Materials Division, 1401 East Broad Street, Richmond, VA 23219, USA.

† Electronic Supplementary Information (ESI) available

References:

1   B. J. Finlayson-Pitts and J. N. Pitts, Chemistry of the Upper and Lower Atmosphere: Theory, Experiments, and Applications; Academic Press, San Diego, CA, 2000.

2   H. Xiao, S. Maeda and K. Morokuma, J. Phys. Chem. Lett., 2011, **2**, 934.

3   D. J. Stewart, S. H. Almabrok, J. P. Lockhart, O. M. Mohamed, D. R. Nutt, C. Pfrang and G. Marston, Atmos. Environ., 2013, **70**, 227.

4   R. P. Wayne, I. Barnes, P. Biggs, J. P. Burrows, C. E. Canosamas, J. Hjorth, G. Lebras, G. K. Moortgat, D. Perner, G. Poulet, G. Restelli and H. Sidebottom, Atmos. Environ. A-Gen., 1991, **25**, 1.

5   S. S. Brown and J. Stutz, Chem. Soc. Rev., 2012, **41**, 6405.

6   J. Kerdouci, B. Picquet-Varrault, R. Durand-Jolibois, C. Gaimoz and J.-F. Doussin, J. Phys. Chem. A, 2012, **116**, 10135.

7   A. Mellouki, G. Le Bras and H. Sidebottom, Chem. Rev., 2003, **103**, 5077.

8   G. B. Ellison, A. F. Tuck and V. Vaida, J. Geophys. Res., 1999, **104**, 11633.

9   T. Novakov, C. E. Corrigan, J. E. Penner, C. C. Chuang, O. Rosario and O. L. M. Bracero, J. Geophys. Res., 1997, **102**, 21307.

10 J. W. Lu, J. M. Flores, A. Lavi, A. Abo-Riziq and Y. Rudich, Phys. Chem. Chem. Phys., 2011, **13**, 6484.

11 J. F. Noxon, R. B. Norton and E. Marovich, Geophys. Res. Lett., 1980, **7**, 125.

12 A. M. Winer, R. Atkinson and J. N. Pitts, Science, 1984, **224**, 156.

13 U. Platt, G. LeBras, G. Poulet, J. P. Burrows and G. Moortgat, Nature, 1990, **348**, 147.

14 J. Eberhard and C. J. Howard, J. Phys. Chem. A, 1997, **101**, 3360.

15 D. Asaf, E. Tas, D. Pedersen, M. Peleg and M. Luria, Environ. Sci. Technol., 2010, **44**, 5901.

This journal is © The Royal Society of Chemistry 2014

Phys. Chem. Chem. Phys., 2014, **00**, 1-3 | **11**

16 Y. Gai, W. Wang, M. Ge, H. G. Kjaergaard, S. Jørgensen and L. Du, Atmos. Environ., 2013, **77**, 696.

17 R. Atkinson, S. M. Aschmann, A. M. Winer and J. N. Pitts, Environ. Sci. Technol., 1985, **19**, 159.

18 I. Barnes, V. Bastian, K. H. Becker and Z. Tong, J. Phys. Chem., 1990, **94**, 2413.

19 R. Atkinson, C. N. Plum, W. P. L. Carter, A. M. Winer and J. N. Pitts, J. Phys. Chem., 1984, **88**, 1210.

20 S. M. Aschmann and R. Atkinson, J. Phys. Chem. A, 2011, **115**, 1358.

21 M. Salgado, M. Gallego-Iniesta, M. Martín, A. Tapia and B. Cabañas, Environ. Sci. Pollut. R., 2011, **18**, 940.

22 K. Wang, M. F. Ge and W. G. Wang, Chem. Phys. Lett., 2010, **490**, 29.

23 Z. J. Zhao, S. Husainy and G. D. Smith, J. Phys. Chem. A, 2011, **115**, 12161.

24 M. D. King, C. E. Canosa-Mas and R. P. Wayne, Phys. Chem. Chem. Phys., 1999, **1**, 2231.

25 A. Tapia, F. Villanueva, M. S. Salgado, B. Cabañas, E. Martínez and P. Martín, Atmos. Chem. Phys., 2011, **11**, 3227.

26 U. W. a. C. Goeschen, Aust. J. Chem., 2011, **64**, 833.

27 S. Gross, R. Iannone, S. Xiao and A. K. Bertram, Phys. Chem. Chem. Phys., 2009, **11**, 7792.

28 S. Gross and A. K. Bertram, J. Geophys. Res., 2009, **114**, 1.

29 J. C. Love, L. A. Estroff, J. K. Kriebel, R. G. Nuzzo and G. M. Whitesides, Chem. Rev., 2005, **105**, 1103.

30 B. D. Gates, Q. Xu, M. Stewart, D. Ryan, C. G. Willson and G. M. Whitesides, Chem. Rev., 2005, **105**, 1171.

31 R. G. Nuzzo, B. R. Zegarski and L. H. Dubois, J. Am. Chem. Soc., 1987, **109**, 733.

32 C. A. Widrig, C. A. Alves and M. D. Porter, J. Am. Chem. Soc., 1991, **113**, 2805.

33 A. Ulman, J. E. Eilers and N. Tillman, Langmuir, 1989, **5**, 1147.

34 L. H. Dubois and R. G. Nuzzo, Annu. Rev. Phys. Chem., 1992, **43**, 437.

35 T. Moise, R. K. Talukdar, G. J. Frost, R. W. Fox and Y. Rudich, J. Geophys. Res., 2002, **107**, 4014.

36 H. Skov, T. Benter, R. N. Schindler, J. Hjorth and G. Restelli, Atmos. Environ., 1994, **28**, 1583.

37 J. Hjorth, C. Lohse, C. J. Nielsen, H. Skov and G. Restelli, J. Phys. Chem., 1990, **94**, 7494.

38 M. Shiraiwa, U. Poschl and D. A. Knopf, Environ. Sci. Technol., 2012, **46**, 6630.

39 Z. J. Zhao, S. Husainy, C. T. Stoudemayer and G. D. Smith, Phys. Chem. Chem. Phys., 2011, **13**, 17809.

40 J. Hu and M. A. Fox, J. Org. Chem., 1999, **64**, 4959.

41 F. Heintz, U. Platt, H. Flentje and R. Dubois, J. Geophys. Res., 1996, **101**, 22891.

42 W. B. DeMore, S. P. Sander, D. Golden, R. Hampson, M. J. Kurylo, C. Howard, A. Ravishankara, C. Kolb and M. Molina, Chemical kinetics and photochemical data for use in stratospheric modeling; JPL Pub., 1994.

43 J. Gorham, B. Smith and D. H. Fairbrother, J. Phys. Chem. C, 2007, **111**, 374.

44 J. Vegh, J. Electron Spectrosc. Relat. Phenom., 1988, **46**, 411.

45 J. Vegh, Surf. Sci., 2004, **563**, 183.

46 J. Baltrusaitis, P. M. Jayaweera and V. H. Grassian, Phys. Chem. Chem. Phys., 2009, **11**, 8295.

47 O. Rosseler, M. Sleiman, V. N. Montesinos, A. Shavorskiy, V. Keller, N. Keller, M. I. Litter, H. Bluhm, M. Salmeron and H. Destaillats, J. Phys. Chem. Lett., 2013, **4**, 536.

48 Gaussian 09, Revision D.01, Frisch, M. J.; Trucks, G. W.; Schlegel, H. B.; Scuseria, G. E.; Robb, M. A.; Cheeseman, J. R.; Scalmani, G.; Barone, V.; Mennucci, B.; Petersson, G. A.; Nakatsuji, H.; Caricato, M.; Li, X.; Hratchian, H. P.; Izmaylov, A. F.; Bloino, J.; Zheng, G.; Sonnenberg, J. L.; Hada, M.; Ehara, M.; Toyota, K.; Fukuda, R.; Hasegawa, J.; Ishida, M.; Nakajima, T.; Honda, Y.; Kitao, O.; Nakai, H.; Vreven, T.; Montgomery, J. A., Jr.; Peralta, J. E.; Ogliaro, F.; Bearpark, M.; Heyd, J. J.; Brothers, E.; Kudin, K. N.; Staroverov, V. N.; Kobayashi, R.; Normand, J.; Raghavachari, K.; Rendell, A.; Burant, J. C.; Iyengar, S. S.; Tomasi, J.; Cossi, M.; Rega, N.; Millam, N. J.; Klene, M.; Knox, J. E.; Cross, J. B.; Bakken, V.; Adamo, C.; Jaramillo, J.; Gomperts, R.; Stratmann, R. E.; Yazyev, O.; Austin, A. J.; Cammi, R.; Pomelli, C.; Ochterski, J. W.; Martin, R. L.; Morokuma, K.; Zakrzewski, V. G.; Voth, G. A.; Salvador, P.; Dannenberg, J. J.; Dapprich, S.; Daniels, A. D.; Farkas, Ö.; Foresman, J. B.; Ortiz, J. V.; Cioslowski, J.; Fox, D. J. Gaussian, Inc., Wallingford CT, 2009.

49 NIST Chemistry WebBook: 2011.

50 R. G. Snyder, H. L. Strauss and C. A. Elliger, J. Phys. Chem., 1982, **86**, 5145.

51 R. G. Greenler, J. Chem. Phys., 1966, **44**, 310.

52 L. Duan and S. J. Garrett, Langmuir, 2001, **17**, 2986.

53 J. W. Lu, L. R. Fiegland, E. D. Davis, W. A. Alexander, A. Wagner, R. D. Gandour and J. R. Morris, J. Phys. Chem. C, 2011, **115**, 25343.

54 J. S. Peanasky and R. L. McCarley, Langmuir, 1998, **14**, 113.

55 M. Wandas and A. Puszko, Chem. Heterocycl. Compd. (N. Y., NY, U. S.), 2000, **36**, 796.

56 C. M. Aubuchon, K. D. Rector, W. Holmes and M. D. Fayer, Chem. Phys. Lett., 1999, **299**, 84.

57 J. Noda, M. Hallquist, S. Langer and E. Ljungstrom, Phys. Chem. Chem. Phys., 2000, **2**, 2555.

58 A. K. Rappe, C. J. Casewit, K. S. Colwell, W. A. Goddard and W. M. Skiff, J. Am. Chem. Soc., 1992, **114**, 10024.

59 W. D. Cornell, P. Cieplak, C. I. Bayly, I. R. Gould, K. M. Merz, D. M. Ferguson, D. C. Spellmeyer, T. Fox, J. W. Caldwell and P. A. Kollman, J. Am. Chem. Soc., 1995, **117**, 5179.

60 D. A. Knopf, J. Mak, S. Gross and A. K. Bertram, Geophys. Res. Lett., 2006, **33**, L17816.

61 J. Jee and F.-M. Tao, J. Phys. Chem. A, 2006, **110**, 7682.

62 D. Zemlyanov and R. Schlogl, Surf. Sci., 2000, **470**, L20.

63 E. I. Vovk, A. Turksoy, V. I. Bukhtiyarov and E. Ozensoy, J. Phys. Chem. C, 2013, **117**, 7713.

64 A. Krepelova, J. Newberg, T. Huthwelker, H. Bluhm and M. Ammann, Phys. Chem. Chem. Phys., 2010, **12**, 8870.

65 K. Heister, M. Zharnikov and M. Grunze, Langmuir, 2001, **17**, 8.

66 A. J. Wagner, S. R. Carlo, C. Vecitis and D. H. Fairbrother, Langmuir, 2002, **18**, 1542.

67 J. Torres, C. C. Perry, S. J. Bransfield and D. H. Fairbrother, J. Phys. Chem. B, 2002, **106**, 6265.

68 A. J. Wagner, S. R. Carlo, C. D. Vecitis and H. Fairbrother, Langmuir, 2002, **18**, 1542.

69 A. D. Vogt, T. Han and T. P. Beebe, Langmuir, 1997, **13**, 3397.

12 | *Phys. Chem. Chem. Phys.*, 2014, **00**, 1-3

This journal is © The Royal Society of Chemistry 2014

70 C. D. Wagner, W. M. Riggs, L. E. Davis, J. F. Moulder and G. E. Muilenberg, Handbook of X-ray Photoelectron Spectroscopy; Perkin-Elmer Corporation, 1979.

71 S. Xiao and A. K. Bertram, Phys. Chem. Chem. Phys., 2011, **13**, 6628.

72 D. J. Donaldson, B. T. Mmereki, S. R. Chaudhuri, S. Handley and M. Oh, Faraday Disc. Chem. Soc., 2005, **130**, 227.

73 R. C. Chapleski, J. R. Morris and D. Troya, Phys. Chem. Chem. Phys., 2014.

80x39mm (300 x 300 DPI)